A role for vocal rhythm in avian speciation

Matteo Sebastianelli
  University of Cyprus

Sifiso Lukhele
  University of Cyprus

Simona Secomandi
  University of Cyprus

Stacey de Souza
  University of Cyprus

Bettina Haase
  The Rockefeller University

Michaella Moysi
  University of Cyprus

Christos Nikiforou
  University of Cyprus

Alexander Hutfluss
  Ludwig-Maximilians University of Munich

Jacquelyn Mountcastle
  The Rockefeller University

Jennifer Balacco
  Rockefeller University

Sarah Pelan
  Wellcome Sanger Institute, Wellcome Trust Genome Campus

William Chow
  Wellcome Sanger Institute

Olivier Fedrigo
  The Rockefeller University

Colleen Downs
  University of KwaZulu-Natal   https://orcid.org/0000-0001-8334-1510

Ara Monadjem
  ara@uniswa.sz   https://orcid.org/0000-0003-1906-4023

Niels Dingemanse
  Ludwig Maximilians University of Munich

Erich Jarvis
  Rockefeller University   https://orcid.org/0000-0001-8931-5049

Alan Brelsford

University of California, Riverside

Bridgett vonHoldt

Princeton University   https://orcid.org/0000-0001-6908-1687

Alexander Kirschel

kirschel@ucy.ac.cy

University of Cyprus   https://orcid.org/0000-0003-4379-7956

Article

Keywords:

Additional Declarations: There is **NO** Competing Interest.

Title: A role for vocal rhythm in avian speciation

Authors:

Matteo Sebastianelli[1], Sifiso M. Lukhele[1], Simona Secomandi[1], Stacey G. de Souza[1], Bettina Haase[2], Michaella Moysi[1], Christos Nikiforou[1], Alexander Hutfluss[3], Jacquelyn Mountcastle[2], Jennifer Balacco[2], Sarah Pelan[4], William Chow[4], Olivier Fedrigo[2], Colleen T. Downs[5], Ara Monadjem[6,7], Niels J. Dingemanse[3], Erich D. Jarvis[2,8,9], Alan Brelsford[10], Bridgett M. vonHoldt[11], and Alexander N. G. Kirschel[1*]

Affiliations:

[1] *Department of Biological Sciences, University of Cyprus, PO Box 20537, Nicosia 1678, Cyprus*

[2] *Vertebrate Genome Lab, The Rockefeller University, New York, NY, USA*

[3] *Behavioural Ecology, Department of Biology, Ludwig-Maximilians University of Munich (LMU), 82152, Planegg-Martinsried, Germany*

[4] *Wellcome Sanger Institute, Cambridge, UK*

[5] *Centre for Functional Biodiversity, School of Life Sciences, University of KwaZulu-Natal, Pietermaritzburg, South Africa*

[6] *Department of Biological Sciences, University of Eswatini, Kwaluseni, Eswatini*

[7] *Mammal Research Institute, Department of Zoology & Entomology, University of Pretoria, Private Bag 20, Hatfield, 0028, Pretoria, South Africa*

[8] *Laboratory of Neurogenetics of Language, The Rockefeller University, New York, NY, USA*

[9] *Howard Hughes Medical Institute, Chevy Chase, MD, USA*

[10] *Department of Evolution, Ecology and Organismal Biology, University of California Riverside, Riverside, CA 92521, USA*

[11] *Department of Ecology & Evolutionary Biology, Princeton University, Princeton, NJ, 08544, USA*

*Corresponding author. Email: kirschel@ucy.ac.cy

Abstract

Bird song mediates speciation but little is known about its genetic basis because of the confounding effect of vocal learning in model systems. Rhythm, in particular, transcends acoustic communication across the animal kingdom and plays a fundamental role in sexual selection and species recognition in birds. Here we investigated the genomic underpinnings of rhythm in vocal non-learning *Pogoniulus* tinkerbirds using a reference we assembled and 134 further individual whole genomes distributed across a Southern African hybrid zone. We show that rhythm speed is associated with two genes that affect speech in humans, Neurexin-1 and Coenzyme Q8A. Leveraging ancestry, we find that rhythmic stability is also associated with these candidate loci. Furthermore, a pattern of character displacement in rhythmic stability in the contact zone suggests there is reinforcement against hybridization, supported by evidence of assortative mating. Assortative mating is asymmetric, however, occurring only in the species that produces faster, more stable rhythms. Rhythmic stability reflects motor performance, a trait long regarded as an indicator of quality. Because rhythm is an omnipresent trait in animal communication, candidate genes shaping vocal rhythm identified here may play a pivotal role in speciation across birds and other vertebrates.

Introduction:

Rhythm enriches human culture and constitutes an essential component of animal communication that mediates species and individual recognition, courtship and mate choice[1,2]. While comparative approaches have contributed towards a better understanding of the functions of rhythm processing[2–4], it is less clear which mechanisms drive differences in rhythm among populations and how these are maintained over time. Rhythm reflects motor performance[5], a trait long considered an indicator of quality for choosy females. As a consequence, mate choice may maintain distinct rhythms through assortative mating, the tendency to mate with individuals of similar phenotype. Assortative mating maintains pre-mating isolation between incipient species[6,7], and therefore plays an essential role in speciation. Despite mounting evidence that supports the role of bird song in driving speciation as a consequence of assortative mating[8–10], relatively little is known about its genetic underpinnings. Most molecular work on bird song has focused on the genetic basis of vocal learning in parrots, hummingbirds and songbirds[11,12]. Because of the confounding effect of cultural vocal learning in these study systems, little is known about the molecular mechanisms underlying the temporal patterning of bird song. Hence, we investigated the genetic basis of bird song rhythm in two vocal non-learning species of *Pogoniulus* tinkerbirds, African barbets (Piciformes: Lybiidae), that are widely distributed across Sub-Saharan Africa (Fig. 1a) and emit remarkably simple rhythmic songs. Their songs comprise a repetitive series of rhythmic pulses delivered at constant pitch and rate, with the latter differing subtly but unambiguously between two species, yellow-fronted tinkerbird (*P. chrysoconus extoni,* hereafter *extoni*) and red-fronted tinkerbird (*P. pusillus pusillus,* hereafter *pusillus*) (Fig. 1b, Supplementary Movies 1-3). Furthermore, Southern African populations of *extoni* and *pusillus* hybridize extensively when they come into secondary contact[13] (Fig. 1c-d). Due to the simple structure of the vocal phenotype that is divergent between the two species and potentially dominant inheritances in admixed individuals[14], this system provides the opportunity for a genome-wide association study (GWAS)[15,16] to identify the genetic basis of vocal rhythm.

Bird song frequency has a tight relationship with body mass[17,18], including in tinkerbirds[19], and is likely polygenic[20]. Temporal features of song such as pulse rate, by contrast, may involve signal transduction, neural regulation or physiological constraints of the syrinx or lungs[21]. Although rhythmic components have been described in birds[2], humans[22] and non-human primates[23], it is only in humans that a molecular basis of rhythmic ability has been identified[22]. Here, we quantified rhythmicity in tinkerbird song by investigating the

3

35   presence of categorical rhythms[2], and explored the relationship between the inter-onset

36   interval (IOI, the time-interval between the onset of consecutive pulses and thus a measure of

37   pulse rate), genotype, and inferred global species-ancestry using a newly assembled

38   chromosome-level reference genome of *pusillus*. We leveraged genomewide and candidate

39   gene-specific local ancestry to determine the relative effects on rhythm rate and stability.

40   Lastly, we characterized the extent of assortative mating in the hybrid zone. We identified a

41   cluster of genes on one chromosome associated with pulse rate, including two genes

42   previously associated with vocal dysfunctions in humans. We further found that locally-

43   inferred genetic ancestry at these loci was also associated with rhythmic stability. A striking

44   pattern of asymmetric nonrandom mating in the contact zone suggests a preference for faster,

45   more stable songs in one species maintains phenotypic distinctiveness despite ongoing gene

46   flow. Our findings support a role for genes shaping vocal rhythm in sexual selection and

47   speciation.

48

49   **[FIG. 1]**

50

51   **Results**

52   **Categorical rhythms and the genomic basis of rhythm in tinkerbirds**

53   Using 80,019 IOI measurements taken from recordings of 124 allopatric individuals,

54   we calculated the rhythmic ratios ($R_k = IOI_k/(IOI_K + IOI_{K+1})$ for *extoni* (n = 81) and *pusillus*

55   (n = 43). Although mean IOI differed significantly between the two species (*extoni* = ~ 0.57 s

56   (± 0.06 SD), *pusillus* = 0.46 s (± 0.02 SD) t-test: $t = 338.04$, $df = 65517$, $P = < 0.001$), their

57   R_k did not differ (t-test: $t = 0.72$, $df = 22166$, $P = 0.468$), with *extoni* $R_k = 0.50$ (± 0.01 SD)

58   and *pusillus* $R_k = 0.50$ (± 0.008 SD). Tinkerbird songs are isochronous with IOI reflecting the

59   on-integer 1:1 ratio (Supplementary Fig. 1), similar to a metronome's tempo[24], demonstrating

60   that pulses are delivered at intervals of identical duration.

61   We assembled a chromosome-level reference genome for a female *pusillus* (GenBank

62   accession number: GCA_015220805.1) using the Vertebrate Genomes Project (VGP)

63   pipeline v1.6. This included a combination of PacBio CLR long reads, 10x Genomics linked-

64   reads, Bionano optical maps, and Hi-C data[25] (see Methods). The final assembly was 1.27 Gb

65   in length (Supplementary Fig. 2a; Supplementary Table 1). We produced an assembly with a

66   scaffold NG50 of 26 Mb and N50 of 34 Mb (Supplementary Table 2), a contig N50 of 16.8

67   Mb, and a per-base consensus accuracy (QV)[26] of 42.8 (~0.53 base errors/10 Kbp;

68   Supplementary Table 3). The assembly has a GC content of 46.0% (Fig. 2), a repeat content

4

69   of 47.3% , a functional completeness[27] of 95.2% (Supplementary Table 4) and a *k*-mer

70   completeness[26] of 85.2% (93.9% when combined with the alternate assembly; Supplementary

71   Fig. 2b; Supplementary Table 3). We assigned 97.8% of assembled sequences to 44

72   autosomes and the sex chromosomes, Z and W (2n = 90; Fig. 2, Supplementary Fig. 2c). The

73   karyotype is concordant with other Piciformes[28].

74

75   **[FIG. 2]**

76

77   We collected whole genome sequence data with an average 8.2-fold coverage from

78   138 colour-banded tinkerbirds that were aligned to our newly assembled reference genome

79   using BWA-MEM[29] and 19.6 million single nucleotide polymorphisms (SNPs) were

80   discovered using GATK4[30]. We conducted a GWAS using a mixed model implemented in

81   GEMMA[31] to identify non-random associations between IOI and SNPs generated for 87

82   individuals in the hybrid zone. We discovered that a single genomic region was associated

83   with IOI variation (Fig. 3a). This region spans approximately 13 Mb of chromosome 25 (Fig.

84   3b-c) and is defined by 15 significantly associated SNPs (-log10P > 6) including 3 that

85   passed a threshold of -log10P > 7 (Supplementary Table 5). We annotated these outlier SNPs

86   by aligning the tinkerbird reference to the annotated zebra finch (*Taeniopygia guttata*)

87   reference (RefSeq assembly accession: GCF_003957565.2) with BLAST[32]. All 15 significant

88   SNPs mapped onto zebra finch chromosome 3, with three SNPs annotated in introns of

89   Neurexin 1 (*NRXN1*), one SNP in an exon of Coenzyme Q8A (*COQ8A*), one SNP in an

90   intron of ENAH actin regulator (*ENAH*), and one SNP in an intron of MutS homolog 2

91   (*MSH2*) (Fig. 3b; Supplementary Table 6). Of these genes, *NRXN1* and *COQ8A* have both

92   previously been associated with human speech disorders[33–35], and *ENAH* with hearing

93   disability[36,37]. *MSH2* has not yet been associated with any vocal communication-related

94   function, although it is mostly expressed in the cerebral cortex and nasopharynx in humans

95   (www.proteinatlas.org)[38]. Given the pattern of variance partitioning, there is likely an uneven

96   contribution from each of the four candidate genes (Fig. 3d), with three genes (*NRXN1,*

97   *COQ8A,* and *MSH2*) each providing significantly greater contributions to total trait variance

98   than *ENAH* and 10,000 randomly selected SNPs across the genome (Supplementary Table 7).

99   Besides these four primary candidate genes, we highlight five additional SNPs identified in

100   the GWAS as possible candidate loci: a single SNP located 69 bp upstream of an undescribed

101   gene whose zebra finch orthologs are yet to be identified (LOC115494518), one SNP within

102   1 Kb from anaplastic lymphoma kinase (*ALK*), two SNP loci located approximately 9.4 and

5

103 15.3 Kb from Forkhead box N2 (*FOXN2*), and one SNP located 9.8 Kb from echinoderm

104 microtubule-associated protein like-4 (*EML4*).

105 We evaluated the ability of the candidate SNPs to accurately predict the vocal

106 phenotype with a Bayesian sparse linear mixed model. Using leave-one-out cross-validation,

107 we found that the predicted and observed IOI trait values were highly correlated (Pearson's R

108 = 0.78) and that the inferred phenotypes explained a statistically significant proportion of

109 observed IOIs (LM: β = 2.04, st. error = 0.17, t = 11.53, P = < 0.001, adjusted R^2 = 0.6;

110 Supplementary Fig. 3). Due to the known critical functions of some candidate genes in

111 human speech[34,35], we calculated long-range haplotype statistics to identify potential

112 signatures of directional selection. We estimated cross-population extended haplotype

113 homozygosity[39] on allopatric individuals of either parent species but found that no significant

114 SNP deviated beyond the 2.5 % and 97.5 % quantiles of the score distribution. However,

115 most SNPs carried a negative value, which is consistent with asymmetric selection in *pusillus*

116 (Fig. 3e).

117

118 **[Fig. 3]**

119

120 **Low genomic divergence in candidate gene region**

121 Despite the congregation of significant SNPs on tinkerbird chromosome 25, chromosome-

122 wide differentiation was low between allopatric *extoni* and *pusillus* (D_{XY} = 0.01±0.002 and

123 F_{ST} = 0.22±0.12) (Fig. 3f-h), when compared to genome-wide means (D_{XY} = 0.01±0.003 and

124 F_{ST} = 0.27±0.16). However, higher relative F_{ST} and D_{XY} occurred together where *NRXN1*

125 SNPs were located, suggesting reduced gene flow at this candidate locus. Nucleotide

126 diversity is higher in *extoni* (Supplementary Fig. 4; Supplementary Table 8). Yet, we found

127 little evidence of linkage disequilibrium, with mean r^2 = 0.09 on chromosome 25 (mean

128 genome-wide r^2 = 0.11) (Supplementary Fig. 5), suggesting that the SNPs in the four

129 candidate genes associated to IOI may not have been inherited together as a linkage group. In

130 addition, four SNP genotypes were fixed in allopatric populations of *pusillus* and three in

131 *extoni* but all were variable in sympatry; IOI reflected underlying genotypes at those loci

132 (Fig. 3i, Supplementary Fig. 6). Sigmoidal geographic clines for genome-wide and gene-

133 specific ancestry confirmed their association with IOI (Supplementary Fig. 7). Although there

134 was detectable population structure between *extoni* and *pusillus* when found in allopatry, the

135 extent of genomic admixture in the contact zone was evident in both the principal component

136 analysis (PCA) and ADMIXTURE (Fig. 1c, 1d). A PCA of the SNPs associated with each

137   candidate gene separately revealed three discrete clusters, one of which carried mostly the

138   heterozygous genotype at candidate loci (Supplementary Fig. 8). The PCA also revealed

139   higher genomic variability in *extoni* with respect to *pusillus*.

140

141   **Ancestry and rhythm**

142   We inferred genome-wide global and local ancestry of 99 individuals sampled from within

143   the geographic hybrid zone, which ranged from one parental type (*extoni* $Q_{pusillus}$ = 0.03) to

144   the other (*pusillus* $Q_{pusillus}$ = 0.99) (Fig. 4a). We estimated a mean of 60±36% *pusillus*

145   ancestry with genomes structured as a mosaic of ancestry blocks (Fig. 4b). Further

146   corroborating the association we report between IOI and specific SNPs, we find a relationship

147   between genome-wide ancestry and IOI (Fig. 3h). This relationship was confirmed in linear

148   mixed models (LMMs) in *glmmTMB*[40], which also confirmed no effect of sex and showed

149   that higher proportions of autosomal and Z-linked *pusillus* ancestry were significantly

150   associated with faster songs (Fig 4c; Supplementary Table 9).

151

152   **[Fig. 4]**

153

154   We then compared the respective ancestry in candidate genes that influence IOI with

155   genome-wide ancestry by fitting genomic clines on allele frequencies of significant SNPs that

156   approach fixation in both allopatric populations (i.e. *NRXN1* and *COQ8A*). We found that the

157   SNPs of both genes undergo a steep shift in allele frequency above a 0.2 proportion of

158   *pusillus* ancestry (Fig. 4d). We next fitted double-hierarchical generalized linear models

159   (DHGLMs) to assess how ancestry proportions affect IOI and its residual within-individual

160   variance (RWV, i.e., level of instability). In addition to modelling a linear effect of ancestry

161   on stability, we also modelled quadratic effects on RWV to test the hypothesis that

162   hybridization results in less stable rhythmic song in admixed individuals. Consistent with the

163   LMMs, greater *pusillus* ancestry was significantly associated with faster songs and negatively

164   with IOI RWV. This corresponds with more stable (i.e., less variance within) songs with

165   increasing *pusillus* ancestry. However, the quadratic effect of ancestry on IOI RWV was not

166   significant, but suggested higher variance (i.e., increased instability) with intermediate

167   ancestry (Fig. 5a, Supplementary Table 10a-c).

168   But we found that specific candidate genes affect song rhythm, and thus predicted that

169   ancestry at those loci rather than genome-wide ancestry would more likely affect song

170   stability. We tested for the effects of local ancestry proportions within the physical regions

that contain the candidate genes associated with IOI. We averaged the ancestry proportion (Q) across all SNPs within the boundaries of the candidate genes and replicated the above model. We found that increasing proportions of *pusillus* ancestry at all four candidate genes was significantly associated with faster and more stable songs (Fig. 5b, Supplementary Table 10d-g). However, for genes *NRXN1* and *COQ8A* we found a significant quadratic effect on RWV that suggests individuals with admixture at these genes sing less stable songs. *Post hoc* analyses further suggested that individuals with higher *pusillus* ancestry at *NRXN1* and *COQ8A* are more sensitive to shifts in ancestry at these two genes. By contrast, individuals with primarily *extoni* ancestry, with increasing *pusillus* ancestry in *NRXN1* before the statistical peak of RWV, have consistent IOI but with increasing variance. For *COQ8A*, the pre-peak effect was negative and marginally significant, suggesting increasing IOI with *extoni* ancestry but with a weaker effect from the statistical peak (Supplementary Fig. 9, Supplementary Table 11).

Character displacement in song stability in sympatry

Intermediate or mixed song might drive reinforcement against hybridization[41]. We explored this possibility by testing for evidence of character displacement in IOI and its stability between 87 pure *extoni* and 94 *pusillus* individuals (respective ancestry > 99%, based on fastSTRUCTURE ancestry values from ddRAD, see Methods). Reproductive character displacement would be manifested in greater differences between the species in IOI or its variance in sympatry compared to allopatry. Instead of divergence in IOI, we found both species sang slower songs in sympatry. However, *extoni* emitted significantly less stable songs in sympatry than in allopatry, and we found a striking interaction effect of a greater difference in rhythmic stability between pure *pusillus* and pure *extoni* in sympatry compared with allopatry (Fig. 5c; Supplementary Table 12). These findings suggest that there is asymmetric reinforcement against hybridization in *pusillus* that is driven by female *pusillus* mating assortatively with *pusillus* males, which have more stable songs than *extoni* and admixed males.

Introgression is asymmetric in the tinkerbird hybrid zone

We investigated possible asymmetric assortative mating by quantifying the direction of gene flow within the contact zone using 82,950 SNPs from ddRAD (mean depth = 13.92X, see Methods). We hypothesized that the presence of contrasting ancestry proportions between sex chromosomes and autosomes could reveal the direction of gene flow in hybridizing

205 populations[42]. We bioinformatically inferred sex by calculating Z chromosome to autosome

206 depth ratios (Supplementary Fig. 10). Then in females, the heterogametic sex in birds, we

207 inferred paternal genome-wide ancestry from their paternally-inherited Z chromosome

208 ancestry. Using the paternal ancestry estimate for 95 females we calculated maternal ancestry

209 from each female's autosomal ancestry (see Methods). There was clear evidence of

210 asymmetric nonrandom mating (LM, $z = 6.949$, $P < 0.001$) (Fig. 5d, Supplementary Table

211 13), consistent with previous findings revealing asymmetric introgression[14]. All 16 mothers

212 with $Q_{pusillus} > 0.97$ mated with males with high *pusillus* proportions ($Q_{pusillus} > 0.83$, mean

213 difference in parental ancestry $\Delta = 0.04\pm0.06$). By contrast, 14 mothers with $Q_{pusillus} < 0.03$

214 (i.e., *extoni* mothers) mated with males whose ancestry varied across the entire range of

215 possible ancestry proportions ($\Delta = 0.62\pm0.34$), between mean ancestry proportions reported

216 above genome-wide (0.6) and of 131 males sequenced with ddRAD from the hybrid zone

217 ($Q_{pusillus} = 0.73\pm0.34$). These results suggest hybridization is asymmetric, with *extoni* females

218 mating with males of any ancestry but *pusillus* females selecting males with high *pusillus*

219 ancestry (i.e., those with faster, more stable songs).

220

221 **[Fig. 5]**

222

223 **Discussion**

224 Our study has revealed the genomic basis of vocal rhythm in tinkerbirds. Of the four

225 candidate genes identified, *NRXN1* and *COQ8A* have been associated with speech and

226 phonology impairments in humans[34]. We highlight *NRXN1*, which studies have linked to

227 several human neurological disorders, including autism[33], but also to alterations in social

228 behaviour, including in male aggressiveness in mice[43], and differences in male-male

229 tolerance in baboons[42]. Here, we found that *NRXN1*, along with *COQ8A,* influenced rhythm

230 speed and stability, and evidence of asymmetric assortative mating suggests a female

231 preference for faster, more stable songs supports a good genes model of sexual selection on

232 male motor performance[44]. The preference for fast, stable song might have evolved in

233 *pusillus* following its divergence from *extoni* and in turn driven asymmetric assortative

234 mating in the hybrid zone, and reinforcement against hybridization. Divergent character

235 displacement has previously been found in tinkerbird song frequency and rate, where it was

236 hypothesized to mediate interspecific aggression between two species that do not

237 interbreed[45,46]. Here, reproductive character displacement in rhythmic stability is a potential

238 mechanism for the maintenance of distinct species phenotypes despite ongoing gene flow.

239   Recent work has supported the hypothesis that speciation occurs even in the presence

240   of gene flow provided some regions in the genome are resistant to introgression[47]. Although

241   we found relatively low differentiation across the chromosome region with the candidate

242   genes, higher relative F_{ST} and D_{XY} occurred where *NRXN1* SNPs were located, suggesting

243   reduced gene flow at candidate loci. But with asymmetric introgression, the effect of

244   assortative mating on reducing gene flow in one species is partly offset by random mating in

245   the other. Nevertheless, with known impacts on human speech[34] and effects on aggressive

246   behaviour in other mammals[42,43], candidate genes identified here may play a wider role in

247   determining pulse rates and rhythmic stability across vertebrates.

248   We also revealed isochronous vocalizations in birds with innate songs, with

249   tinkerbirds delivering notes at equally-spaced time intervals. Isochrony, which has been

250   identified in humans, non-human primates, songbirds and bats[2,23,48], is thought to facilitate

251   acoustic coordination and processing, especially in vocal learners[49]. Tinkerbirds are not vocal

252   learners[50], but contrary to assertions that vocal non-learners lack the ability to perceive

253   isochronous rhythms[51], our study suggests perception of different rhythmical patterns might

254   have driven selection for isochrony even in species with limited vocal flexibility. Indeed,

255   although tinkerbirds do not duet, perception of rhythmic patterning is likely fundamental for

256   acoustic coordination in confamilial vocal non-learner species from independent clades

257   within Lybiidae that perform highly coordinated multi-individual acoustic displays[52]. Vocal

258   rhythm is an omnipresent trait of bird song that functions in species recognition and sexual

259   selection. Our study suggests vocal rhythm plays a pivotal role in pre-mating isolation and

260   speciation, and this is associated with genetic variation in candidate genes that function in the

261   brain.

262

263   **Methods**

264   *Fieldwork*

265   Fieldwork was performed in Eswatini and South Africa between 2015 and 2022 to sample

266   and record the sympatric and allopatric populations of yellow-fronted tinkerbird *Pogoniulus*

267   *chrysoconus extoni* and red-fronted tinkerbird *Pogoniulus pusillus pusillus*. Our sampling

268   efforts focused on the breeding season - the rainy season - to take advantage of the territorial

269   response of breeding pairs. Tinkerbirds were lured into mist nets using conspecific playbacks,

270   measured and provided with a uniquely numbered metal band and a specific combination of

271   color bands prior to release. Blood samples were obtained from each banded individual

through venipuncture of the brachial vein and stored in 1ml queen's lysis buffer (aliquoted

from 800 ml dH2O; 1,22g Tns-Cl; 0,6 NaCl; 200 ml EDTA; 10g n-lauroylsarcosine; pH 8)

for 443 samples or 100% ethanol (1ml × 9 samples). This total included 85 samples obtained

for a previous study[14]. Two samples of *pusillus* were collected with the aim of assembling a

reference genome at Mlawula Game Reserve, Eswatini in July 2019, with blood stored in

100% ethanol and placed on dry ice in the field, before transfer to a -80 °C freezer prior to

shipping to the Vertebrate Genomes Lab, at the Rockefeller University for sequencing. We

visited capture sites repeatedly thereafter, with the aim of locating color-banded tinkerbirds,

which would then be elicited to sing with the use of conspecific playbacks and recorded;

although we also recorded unbanded tinkerbirds as well every time we were presented with

the opportunity. We recorded tinkerbird vocal responses using a Marantz PMD 661 with

either a Sennheiser MKH 8050 directional microphone or MKH 8070 shotgun microphone

and saved recordings as 16-bit WAV files at a sampling frequency of 48 kHz. In total we

sampled 468 tinkerbirds and obtained 710 recordings from 491 individuals across allopatric

and sympatric sites. A subset of these recordings were previously used towards another study

focusing on continent-wide patterns of song frequency[19].

Acoustic analysis

WAV files were imported into Raven Pro[53], where notes were detected using the built-in

band-limited energy detectors (BLED) following a previously established protocol[19,54]. The

BLED detects notes when their amplitude in a pre-defined frequency band exceeds a specific

signal-to-noise ratio (in dB) of background noise. We visually inspected note annotations to

control for missing detections and control for false positives (i.e. sounds of similar structure

to the tinkerbird notes that were detected by the BLED). False positives were deleted from

the annotations, whereas gaps resulting from missed notes were manually filled by fitting a

selection around a note using the waveform view as a reference to avoid errors related to the

visual interpretation of the spectrogram. This procedure was also applied to adjust the

selection box in cases they did not match the exact onset and offset time of a note. We

calculated the difference between the onset times of two consecutive notes to obtain the inter-

onset interval (IOI). We believe that this measurement is a more reliable measure of pulse

rate because it does not take into consideration the end time of a note, which may vary across

recordings and sites as a consequence of differences in attenuation and sound reverberation[55].

This workflow resulted in two datasets, one containing all IOI intervals (hereafter 'All

305 Notes') and one with IOI values averaged across each individual recording (hereafter 'mean

306 IOI').

307

308 *Quantification of rhythmicity in tinkerbirds*

309 To assess rhythmicity in tinkerbird song we quantified categorical rhythms, in which

310 temporal intervals among notes are distributed discretely rather than continuously[23,56]. Such

311 rhythm categories can be identified by calculating rhythmic ratios $(R_k)^2$, in which each IOI

312 value is divided by itself plus the value of the subsequent interval $(R_k = IOI_k/(IOI_K + IOI_{K+1})$.

313 Following this approach, an R_k of 0.5 would equate to a 1:1 rhythm ratio and therefore

314 isochrony, meaning that each note is delivered at an equally spaced interval.

315

316 *Genomic data extraction, library preparation and sequencing*

317 We generated a *de novo* chromosome-level reference genome assembly from a *pusillus*

318 female individual sampled in Mlawula Game Reserve, Eswatini, using four different

319 sequencing technologies: Pacific Biosciences (PacBio) CLR long-reads, 10x Genomics

320 linked-reads, Bionano optical maps and Hi-C reads from Arima Genomics. DNA extraction

321 was performed using a modified protocol of the Bionano Prep SP Frozen Human Blood DNA

322 Isolation Protocol for the Bionano Prep SP Blood and Cell Culture DNA Isolation Kit (cat no.

323 80030). Briefly, the input volume was adjusted to 15 µl of blood and then brought to a total

324 of 40 µl with chilled 1x PBS. The lysis and digestion was performed on the whole blood and

325 PBS mixture. Isolated high molecular weight DNA was kept at room temperature for a week

326 to homogenize before quantified with a Qubit 3 fluorometer (Invitrogen Qubit dsDNA Broad

327 Range Assay cat no. Q32850). DNA fragment size distribution was assessed using a pulsed

328 field gel electrophoresis (PFGE; Pippin Pulse, SAGE Science, Beverly, MA) and found the

329 majority of DNA was over 300 Kb. The obtained DNA was then used to prepare the libraries

330 for the different sequencing technologies. For PacBio libraries, DNA was sheared down to

331 ~40 Kb fragment size by needle shearing. To prepare PacBio large insert libraries, the

332 SMRTbell express template pre kit 2.0 (no. 100-938-900) was used. Using Sage BluePippin

333 (Sage Science, USA), libraries were size-selected for 15 Kb, and were then sequenced on

334 three 8M SMRT cells with the Sequel II instrument, using the Sequel II sequencing kit 2.0

335 (no. 101-820-200) and 15-h movie time.

336 To generate linked reads, the extracted DNA was processed on the 10X Genomics

337 Chromium platform (Genome Library Kit & Gel Bead Kit v2 PN-120258, Genome Chip Kit

338 v2 PN-120257, i7 Multiplex Kit PN-120262) following manufacturer's guidelines. The

libraries were then sequenced on an Illumina NovaSeq 6000 S4 150-bp PE lane at ~60×
coverage. For Bionano libraries, the DNA was labeled using direct labeling enzyme (DLE1)
following the DLS protocols (document number 30206). The samples were then imaged on a
Bionano on a Bionano Saphyr instrument. Finally, chromatin interaction (Hi-C) libraries
were generated by Arima Genomics (https://arimagenomics.com/) from the blood samples
with in vivo cross-linking using the two-enzymes Arima-HiC kit (P/N: A510008). The
proximally ligated DNA was sheared, size-selected around 200-600 bp with SPRI beads, and
enriched for biotin-labeled DNA using streptavidin beads. Illumina libraries were then
generated from the fragments using KAPA Hyper Prep kit (P/N: KK8504) and subsequently
amplified through PCR and purified using SPRI beads. After a quality check with qPCR and
Bioanalyzer, the libraries were sequenced on Illumina HiSeq X at ~60× coverage following
the manufacturer's protocols.

For population genomics analyses, we sequenced 137 further tinkerbirds at the whole-
genome level (Supplementary Table 14) on Illumina NovaSeq 6000 S4 150-bp PE lanes
(median depth = 8.53X; mean depth = 8.21X), of which 52 were assigned to *extoni* and 85
pusillus (including 28 allopatric *extoni* and 12 allopatric *pusillus*) based on forecrown color.
We also sequenced a total of 452 tinkerbird samples, including 123 of those sequenced with
WGS, using double-digest restriction site associated DNA sequencing (ddRAD), 85 of which
were included in a previous study[14] (Supplementary Table 15).

From each sample, 0.4 μg of DNA was used for whole-genome sequencing. Libraries
were generated using the NEBNext DNA Library Prep Kit following the manufacturer's
recommendations. The PCR products were then purified using the AMPure XP system,
analyzed for size distribution (by Agilent 2100 Bioanalyzer) and quantified using real-time
PCR. The libraries obtained with this method were then sequenced with the Illumina
Novaseq6000 platform.

The ddRAD sequencing procedure also involved multiple stages. The first stage
includes digestion of DNA with restriction enzymes (*Sbf*I and *Mse*I). We prepared a first
master mix with the restriction enzymes and then combined the master mix with individual
DNA samples in each plate well. The combination master mix with DNA was then vortexed,
centrifuged and incubated. The following stage was the ligation of barcoded adapters which
included thawing the adaptors, preparation of a second master mix, the addition of this master
mix to each well of the restriction digested DNA and finally the addition of a unique
barcoded adaptor for each DNA sample. The third stage involved purification (removal of
short fragments) using Agencourt AMPure. AMPure purification consists in: i) addition of

373   AMPure beads to the DNA volume, ii) binding, iii) separation of the beads from the solution

374   by placing the reaction plate onto a magnetic plate, iv) ethanol wash by adding a specific

375   amount of ethanol to each well of the plate, v) addition of the elution buffer and vi) transfer

376   of the eluent with DNA into a new plate. Subsequently, the next stage includes the

377   amplification of each individual sample in four separate PCR reactions. This PCR step used

378   the Illumina PCR primers to amplify fragments that have our adapters and barcodes ligated

379   onto the ends. To improve stochastic differences in PCR production of fragments in

380   reactions, we ran four separate reactions per restriction-ligation product to then combine

381   them. We prepared a third master mix with standard PCR reagents including Q5 high-fidelity

382   polymerase, and added the combined master mix III to each plate well followed by the

383   addition of the diluted restriction-ligation purified with AMPure mix. Next, we ran the PCR

384   for 20 thermal cycles. Subsequently, to maximise the amount of double-stranded DNA and

385   reduce DNA heterodimer content, we prepared another master mix (master mix IV) with

386   additional PCR primers and dNTPs, added it to each PCR product and then ran one additional

387   thermal cycle. In the following phase, we evaporated the PCR product to about ½ volume and

388   pooled the PCR product from the four replicates and all samples into one tube. Then we ran

389   the PCR product on an agarose gel and selected fragments between 400 and 500 bp in order

390   to exclude fragments that consist mostly of adaptor sequence. We then conducted a final

391   AMPure cleanup on the pooled library and shipped it to Novogene Inc. for 150 bp paired-end

392   sequencing on an Illumina HiSeq X Ten platform.

393

394   *Chromosome-level reference genome assembly and evaluation*

395   Prior to the assembly, a *k*-mer histogram (31 bp) was generated with Meryl[26] from

396   unassembled 10x linked reads generated for the reference genome individual. The histogram

397   was then used with Genomescope[57] to estimate genome size, heterozygosity and repeat

398   content. The reference genome was assembled with the VGP standard genome assembly

399   pipeline 1.6[25] using the PacBio CLR long reads, 10x linked reads, Bionano optical maps and

400   HiC reads. Briefly, PacBio subreads were assembled into contigs with FALCON[58] v. 1.3.0

401   and haplotypes further phased with FALCON-Unzip[59] v. 1.2.0. A set of primary contigs,

402   representing the principal pseudo-haplotype, and a set of alternate haplotigs, representing the

403   alternate haplotype, were generated. Purge_dups[60] was used on the primary contigs to remove

404   any retained alternate haplotigs, overlaps, collapsed repeats and low- and high-coverage

405   contigs. The alternate haplotigs were merged together in a single file and purged again, while

406   the primary purged contigs were subjected to three steps of scaffolding.

407   The first scaffolding step was performed with Scaff10X v2.0-2.1

408   (https://github.com/wtsi-hpag/Scaff10X) using 10x linked reads to join proximal contigs into

409   larger scaffolds. The resulting set of scaffolds were then scaffolded with Bionano DLS

410   optical maps[61] using Bionano Solve v3.2.1 in non-haplotype assembly mode with a DLE-1

411   one enzyme non-nicking approach. The third and last step of scaffolding was performed

412   aligning the Hi-C reads to the scaffold assembly using the Arima Genomics mapping pipeline

413   (https://github.com/ArimaGenomics/mapping_pipeline) and scaffolded using Salsa2 HiC v.

414   2.2[62].

415   To improve the assembly per-base accuracy (QV)[25], the primary scaffolded assembly

416   was merged with the alternate combined haplotigs and the mitogenome to prevent switches

417   and NUMTs overpolishing[25,63], and three steps of polishing were performed. The first step of

418   polishing was with Arrow v. SMRTLink7.0.1 (PacificBiosciences) using PacBio CLR reads.

419   The last two rounds of polishing were done with Longranges Align v. 2.2.2 and freebayes[64] v.

420   1.3.1 using 10x linked reads. Primary scaffolded assembly and alternate haplotigs were then

421   separated again and called with the prefix 'bPogPus1', on the basis of the VGP guidelines for

422   genome identifiers[25]. Manual curation was then performed on the primary assembly to

423   remove any remaining false duplications, correct structural assembly errors, and assign

424   scaffolds to chromosome names. Curation also included a custom decontamination pipeline[65],

425   the genome browser gEVAL[66] v. 2020-05-14, HiGlass Hi-C 2D maps and pretextView

426   (https://github.com/wtsi-hpag/PretextView)[67] were used. The final curated assembly was

427   evaluated with gfastats[68], Merqury[26] (21bp k-mer) and BUSCO[27] ('aves' BUSCO genes) on

428   the European Galaxy Server[69]. Following Secomandi et $al.$, 2023

429   (https://github.com/SwallowGenomics/BarnSwallow/blob/main/Analyses/assembly_evaluati

430   on/assembly_evaluation.txt)[70], we masked the genome with a combination of Windowmasker

431   v1.0.0[71] and RepeatMasker v4.1.4[72] using the RepBase v20,170,127 database[73].

432
433   *Whole-genome variant calling*

434   To process raw whole-genome sequences of 137 $extoni$ and $pusillus$ we first proceeded to

435   trim Illumina adapter sequences using Cutadapt[74] v. 4.0 and merged pair-end reads to

436   produce single interleaved FASTQ files. We then aligned the reads to the recently

437   assembled reference genome of a female red-fronted tinkerbird ($pusillus$: NCBI BioProject:

438   PRJNA637953) using BWA-mem[29] v. 0.7.1 , and included read group information. We also

439   aligned the raw 10x linked reads of the reference genome individual to the reference for

440   inclusion in subsequent analyses. Subsequently, we used SAMtools[75] v. 1.9 to filter out

441   mapped reads with mapping quality below 20 and sort the data by coordinate before

442   converting SAM to BAM files. We then removed duplicate reads with Picard's

443   MarkDuplicates tool[76] (version 2.23.1). We performed all subsequent processes in GATK[30]

444   v.4.0.11.0. We used HaplotypeCaller for individual-level variant calling, we then combined

445   samples using CombineGVCFs and performed joint genotyping with GenotypeGVCFs. This

446   process resulted in a single VCF file which we then filtered using GATK's recommended

447   hard filtering parameters (QUAL < 30.0, QD < 2.0, SOR > 3.0 , FS > 60.0, MQ < 40.0,

448   MQRankSum < -12.5 and ReadPosRankSum < -8.0) to produce two variant files, one

449   containing SNPs and the other containing indels. We then used these variants to implement

450   base quality score recalibration (BQSR), in which the base quality scores of the BAM files,

451   obtained after removing duplicate reads, were adjusted in a two-step process. Firstly, we

452   used BaseRecalibrator to build a recalibration model for each BAM file along with the

453   variant files previously produced. Secondly, we used ApplyBQSR to adjust the base quality

454   scores within each BAM based on the recalibration model, to produce a new recalibrated

455   BAM file. Additionally, we built a second model from the recalibrated BAMs and produced

456   'before-and-after' plots to visualize the effects of the recalibration process using

457   BaseRecalibrator and AnalyseBQSR, respectively. Using the recalibrated BAMs, we then

458   called variants on an individual level, combined samples and performed joint genotyping, to

459   produce the final VCF file, using the same tools described above. We finally applied filters to

460   create two high-quality datasets for subsequent analyses that have different data

461   requirements. Using VCFtools[77] v. 0.1.16, we first created a filtered dataset with the

462   following parameters: maximum missingness = 0.95; minor allele frequency = 0.03;

463   minimum depth = 3.5 and maximum depth = 50, and then created a second dataset with the

464   same filter parameters excluding the minor allele frequency (hereafter 'no MAF' dataset).

465   The no MAF dataset also contained invariant sites, which were necessary to calculate

466   statistics such as π and D_{XY}, whereas we used the MAF filtered dataset in all the other

467   analyses unless noted. Overall, from the initial pre-filtered vcf files of 65,812,270 and

468   631,918,066 SNPs (with invariant sites), the above-mentioned pipeline resulted in a final

469   dataset of 19,602,343 SNPs for the MAF filtered dataset and 303,114,882 SNPs for the no

470   MAF dataset. Upon further exploration of the whole-genome dataset, we removed two

471   allopatric individuals of each species that we deemed had been mislabelled and another

472   allopatric *extoni* which showed signs of contamination, possibly during DNA extraction, with

473   the final dataset consisting of 135 individuals.

474

475 *Double-digest restriction site associated DNA sequencing (ddRAD)*

476 To investigate the direction of backcrossing, we complemented the whole-genome dataset

477 with ddRADs since most individuals sequenced at the whole-genome level were males. SNPs

478 were called from 452 samples of *extoni* and *pusillus* following a standardized pipeline using

479 Stacks[78] v. 2.62. Firstly, we demultiplexed the raw reads using process_radtags along with a

480 list including barcodes associated with individual samples to produce single sample FASTQ

481 files for each paired-end read. Subsequently, we removed PCR clones using clone_filter. We

482 then mapped and aligned the reads to the *P. p. pusillus* reference genome

483 (bPogPus1.pri.cur.20200514.fasta) using BWA-mem v. 0.7.1. Using SAMtools v. 1.9, we

484 filtered out mapped reads with mapping qualities < 20 and sorted the reads by coordinate

485 before converting from SAM to BAM. Following this, we called variants and genotyped

486 using *gstacks* in Stacks (using *--var-alpha* 0.01 and *--gt-alpha* 0.0)[78]. Lastly, population

487 genetics statistics were obtained using *populations* in Stacks together with a pop.map file

488 specifying the population of each sample. Ultimately, we produced a VCF file with 82,950

489 SNPs after filtering out variants that had a depth < 4, > 20% missing genotype data, and a

490 minor allele frequency < 5%, resulting in a median depth = 12.85X and a mean depth =

491 13.92X.

492

493 *Relative sequence depth sexing*

494 Male birds have two copies of the Z chromosome, while females have one Z and one W

495 chromosome. We therefore compared relative sequence depth of the Z chromosome in each

496 individual to autosome depth, with the expectation that males would have similar Z

497 chromosome to autosome depth with two copies of each, whereas females would have half

498 the depth on the Z compared to autosomes[14]. Using this approach, female individuals should

499 have a depth ratio centered around 0.5, whereas males should have a value of approximately

500 1. Based on the depth ratio distribution, we classified individuals with a *Z:autosome* depth

501 ratio < 0.7 as females and those with a > 0.9 as males.

502

503 *Population structure analysis*

504 To investigate population structure across our samples, we first created an unlinked dataset

505 by pruning our MAF-filtered whole genome dataset to filter for loci within 100 Kb windows

506 distance with an r^2 above 0.1 (using *--indep-pairwise 100 kb 10 0.1*) in PLINK v1.90b3i[79].

507 Principal Components Analysis (PCA) was then conducted on allele frequencies across the

508 entire genome in PLINK using the *--pca* flag. Furthermore, we performed PCA on specific

509   genomic regions identified by the analysis in GEMMA (see *Identifying candidate loci*) to

510   investigate population structuring within the loci that are significantly associated with IOI.

511   For analysis of genome-wide population structure we used ADMIXTURE v1.3[80] and, for

512   consistency with other studies on this Southern African population[13], set the assumed number

513   of populations (i.e. K) equal to 2.

514   We also inferred population structure from our ddRAD dataset by running

515   fastSTRUCTURE[81] . This was done to obtain a measure of ancestry from more individuals

516   within the population and specifically, more females, since only a portion of the total

517   individuals sampled were sequenced at the whole genome level with priority given to color-

518   banded individuals whose songs we recorded,which were mostly males. To determine the

519   direction of introgression in the hybrid zone, which previous studies suggested was

520   asymmetric[14], we needed to focus on the heterogametic sex, i.e. females, because paternal

521   ancestry could be estimated based on the ancestry of the single Z chromosome inherited from

522   the father. To do so, we compared ancestry values calculated in fastSTRUCTURE between

523   the Z chromosome and the autosomes (see *Assessing the direction of backcrossing* for a

524   detailed description).

525

526   *Identifying candidate loci underlying IOI*

527   To identify candidate regions that underpin differences in IOI between *extoni* and *pusillus* we

528   ran linear mixed-effects models (LMMs, using the *-lmm 1* command) in GEMMA v0.98[31].

529   We focused specifically on 87 color-banded individuals recorded and sequenced at the

530   whole-genome level from the contact zone only, to minimize effects of spatial population

531   structuring (i.e. isolation-by-distance) and accounted for potential relatedness among

532   individuals by supplying an estimated relatedness matrix as a covariate in the LMM.

533   GEMMA output was then analyzed and interpreted further based on significant SNPs that

534   passed a significance threshold set by permutation, which was performed by running 999

535   LMMs in GEMMA after shuffling phenotypes at random in each run. We set two thresholds,

536   with the most stringent being the mean value of the most significant SNP from each

537   GEMMA run ($-log_{10}P = 6.9$, rounded to 7) and the less stringent threshold established by

538   averaging the p-value of the 10 most significant SNPs across each run ($-log_{10} P = 6.1$,

539   rounded to 6). We investigated just those clusters with at least three significant SNPs.

540   Clusters of significant SNPs were then located in the *pusillus* reference genome after aligning

541   them to the zebra finch (*Taenopygia guttata*) genome using BLAST[32]. We then performed the

542   reverse process: after identifying potential genes that underlie the expression of IOI, we

18

543 extracted their exact gene position from the annotated zebra finch genome and used BLAST
544 to locate the genes in the tinkerbird genome. Following this, from the GEMMA output we
545 extracted beta values and standard error only for the SNPs in the gene regions where the
546 significant SNPs mapped into in order to calculate their effect size. We then compared the
547 effect sizes of each gene against 10,000 SNPs randomly chosen across the entire genome.
548 This was done by estimating the standard error over the mean (SEM), a measure of the
549 variance explained by each gene. We also predicted IOI values in GEMMA using a leave-
550 one-out cross validation approach in a Bayesian sparse linear mixed model (using the *-predict*
551 *1* flag). This was achieved by excluding the phenotypic information of one individual at a
552 time and using the remaining 86 individuals to predict its phenotype based on their genotype.
553 We then estimated the predictive performance of the inferred IOI by fitting a linear model to
554 assess the proportion of observed IOI variance explained by the predicted IOI values.
555
556 *Efficient Local Ancestry Inference*
557 We further investigated local ancestry for each individual in the contact zone using a two-
558 layer hidden Markov model implemented in the Efficient Local Ancestry Inference (ELAI)
559 software[82]. This approach utilizes linkage disequilibrium within and between parental
560 populations and assigns dosage scores between 0 and 2 (for a two-way admixture model) that
561 reflect ancestry proportions in each SNP in individuals from admixed populations. Dosage
562 scores of 0 and 2 indicate each homozygous state, whereas a dosage score of 1 reveals the
563 heterozygous state.
564 After identifying parental populations based on sampling localities (allopatric sites)
565 and ADMIXTURE scores (see *Population structure analysis*), we applied 2 upper-layer
566 clusters (*-C*) and 10 low-layer clusters (*-c*) (five times the value of *-C*, as recommended in the
567 user's manual). Given the uncertainty related to the timing of the admixture event, we
568 investigated four possible values of the admixture generations parameter (i.e. *-mg*), therefore
569 estimating ancestry scores assuming five, ten, fifteen and twenty generations since the
570 admixture event. For each migration parameter, we ran three independent runs with 30 EM
571 steps (*-s*) and finally averaged the 12 independent runs. We classified sites with allele dosage
572 scores between 0.5 and 1.5 as heterozygous, sites < 0.5 as homozygous for *extoni* and those
573 with scores > 1.5 as homozygous for *pusillus* alleles.
574

Assessing the direction of backcross

576 To estimate possible asymmetry of introgression in the hybrid zone between *extoni* and

577 *pusillus*, we compared the extent of admixture in the autosomes and the Z chromosome

578 separately in 95 females sequenced with ddRADseq using fastSTRUCTURE. By inheriting

579 only one copy of the Z chromosome from their fathers, female birds can be used to determine

580 the direction of backcrossing in hybrids. This can be achieved by comparing the Z

581 chromosome and the autosomal ancestry. Assuming that the Z chromosome ancestry of a

582 female individual reflects her father's Z chromosome ancestry, that her autosomal ancestry is

583 an average of her two parents' ancestry value and that the father's autosomal ancestry equals

584 his Z chromosome ancestry, then the maternal ancestry = (2 x autosomal ancestry) - Z

585 ancestry. Using a similar approach to Sørensen *et al., 2023*[42], we quantified differences in

586 mating preferences by fitting a linear model (LM) using the difference between the calculated

587 ancestries for each parent (Δ parental ancestry) as a response variable and a binary variable

588 for maternal ancestry, pure (<97%) *pusillus* (n = 16) vs. pure (<97%) *extoni* (n = 14) as the

589 predictor, expecting pure *pusillus* mothers to have a significantly lower Δ parental ancestry as

590 a consequence of the more similar ancestry between parents.

591

592 *Genome scans for diversity and linkage*

593 Using the no-MAF dataset with invariant sites, we calculated genome-wide F_{ST}, a relative

594 measure of genetic differentiation, D_{XY}, an absolute measure of genetic differentiation and $π$,

595 nucleotide diversity, between allopatric *extoni* and *pusillus* in 25 kb non-overlapping

596 windows using the *popgenWindows.py* custom script

597 (https://github.com/simonhmartin/genomics_general). For graphical purposes, we also

598 computed genome-wide F_{ST} in 500 kb windows (see Fig. 2) as well as r^2, a measure of

599 linkage disequilibrium (LD). To estimate the latter, we first calculated LD in 25 kb non-

600 overlapping windows and, following Secomandi *et al*., 2023[70], we averaged genome-wide

601 LD values within 500 kb blocks using the *chr_ld.pl* custom script

602 (https://github.com/SwallowGenomics/BarnSwallow/blob/main/Analyses/LD-

603 scripts/chr_ld.pl) to visualize areas of the genome that are in high linkage (see Fig. 2).

604

605 *Genome scans for signatures of selection*

606 Genome-wide diversity statistics such as F_{ST} and D_{XY} can be prone to bias, and are

607 specifically affected by variation in recombination rates across the genome. Hence, we also

608 calculated cross-population extended haplotype homozygosity (xpEHH) in allopatric

609   individuals, a method that compares haplotype lengths between populations to control for

610   local variation in recombination rates[39]. Increasing frequencies of selected alleles result in

611   long haplotypes surrounding the selected allele in a population that underwent the sweep. By

612   comparing the haplotype homozygosity between two lineages, xpEHH can identify regions

613   that have undergone selective sweeps and therefore subject to positive selection. This method

614   therefore allows us to identify genomic signatures of positive selection at those loci

615   underpinning IOI and, by consequence, selection for faster or slower songs. In our case,

616   highly positive values indicate selection in *extoni*, whereas negative values indicate selection

617   in *pusillus*. To calculate xpEHH, we first statistically phased each chromosome in the MAF

618   filtered dataset separately using ShapeIt2 v2.r790[83] and then computed xpEHH across

619   allopatric individuals using the *rehh* package in R[84].

620

621   *Geographic and genomic clines*

622   We fitted sigmoidal geographic clines to assess how variation in IOI and ancestry relates to

623   distance from the contact zone. To do so, we used ArcMap v10.7 to calculate the distance of

624   each data point to a line drawn through the centre of the contact zone. Since such a line

625   extends from East to West, we attributed negative distance values to points south of the

626   contact line and positive distance values to points north of this line. To avoid having large

627   sampling gaps either side of the contact line, for this analysis we also included recordings of

628   unbanded tinkerbirds from allopatric sites. We then fitted geographic clines for IOI and

629   ancestry in the *HZAR* R package[85] following the scripts provided therein. We further fitted

630   binomial genomic clines to investigate changes in allele frequency with ancestry using the

631   *HIest* package[86] after creating a matrix of the genotypes (i.e. AA = 0, AB = 1, BB = 2) of the

632   significant markers associated with IOI.

633

634   *Statistical analysis*

635   We further investigated the relationship between ancestry and IOI by running linear mixed-

636   effects models in the *glmmTMB* R package[40]. These models used the 'mean IOI dataset', with

637   IOI set as a dependent variable and proportion of *pusillus* ancestry (with 0 = pure *extoni* and

638   1 = pure *pusillus*) and sex as fixed effects, since nine individuals we recorded were females.

639   We ran separate models for autosomal and Z-linked proportions of *pusillus* ancestry,with

640   individual ID nested in sampling location as random effects. Model fit was validated using

641   the functions provided in the *DHARMa* package in R[87].

642   We also investigated the relationship between ancestry and IOI from a variance

643   perspective to determine how ancestry may affect the stability of rhythmic song. To achieve

644   this we used univariate double hierarchical generalized mixed model (DHGLMs) to estimate

645   random and fixed effects in both the 'mean' and within-individual residual variance 'RWV'

646   parts of models[88] using *brms* in R[89]. We used the 'All Notes' dataset to investigate the impact

647   of hybridization on tinkerbird IOI, with a particular focus on the effects of mixed ancestry on

648   IOI residual within-individual variance (RWV). We hypothesized that pure ancestry

649   individuals would sing less temporally variable songs, thus their songs would be more stable

650   in IOI. Because tinkerbirds develop their songs innately[50], hybrids might be expected to share

651   acoustic features of both parental species as a consequence of their admixed genomes, thus

652   resulting in less temporally stable song. If hybridization results in less attractive songs as a

653   consequence of its instability, this could reveal a potential mechanism of a post-mating

654   extrinsic barrier reinforcing species differences between related species.

655

656   *Testing for hybrid song instability*

657   To test for the effects of ancestry on song rate and stability, we removed one juvenile

658   hybrid individual whose inconsistent song we deemed an age-related factor. We then

659   modelled IOI as a function of the proportion of *pusillus* ancestry across the entire genome

660   and included individual ID as a random factor. We used the same predictors and random

661   effect in the RWV part of the model with the addition of a quadratic function for *pusillus*

662   ancestry. We did this to model a possible non-linear relationship between variance in IOI and

663   ancestry, with intermediate values of ancestry predicted to have higher RWV than extremes

664   representing pure ancestry of either species if hybrids emitted less stable songs. We compared

665   the widely applicable information criterion (WAIC) for three models. The first model

666   included just a linear effect of ancestry in the variance part to account for the possibility that

667   one species may be more variable than another, as recently found in zebra finches[90], and

668   because asymmetric introgression may be associated with a linear pattern in IOI both in the

669   mean and variance part. The second model was fitted with just the quadratic effect of

670   ancestry to test for non linear relationships between ancestry and IOI (i.e. instability of hybrid

671   individuals), and a final full model included both terms. Moreover, in addition to using whole

672   genome ancestry values, we aimed to pinpoint possible effects in candidate genes by using

673   ancestry proportions from the specific genes associated with IOI in GEMMA that were

674   extracted with BLAST and their ancestry calculated in ELAI.

22

675　　　　　For any model with a significant quadratic effect (i.e. with 95% CI not overlapping

676　　　zero), we also ran an additional *post hoc* analysis in *lme4*[91] to investigate the patterns of the

677　　　quadratic effect, which can occur due to effects occurring prior to the inflection point of the

678　　　quadratic curve, effects after the inflection point of the quadratic curve, or both (i.e. here an

679　　　increase or decrease in IOI variance with higher proportions of *extoni* ancestry, *pusillus*

680　　　ancestry, or both). We therefore estimated the value of IOI variance at the statistical peak

681　　　(IOI RWV peak, the *y* coordinate of the inflection point of the quadratic function) and its

682　　　corresponding ancestry value (ancestry at peak, the *x* coordinate of the inflection point of the

683　　　quadratic effect)[92] to then perform a pre-/post-peak analysis. With β_0 being the intercept of

684　　　the RWV part of the model (also called σ), β_1 the variance (σ) estimate of the linear effect

685　　　and β_2 the σ estimate of the quadratic effect, we calculated the IOI RWV peak as $\beta_0 - \beta_1^2/4\beta_2$

686　　　as well as the ancestry value at the peak $(-\beta_1/2\beta_2)$[93]. We then replaced the quadratic term in

687　　　the original model with two new covariates: 1) a categorical 'pre-peak' variable (with post-

688　　　peak ancestry values coded as "0" and pre-peak values coded as "1") and 2) the interaction

689　　　between 'pre-peak' and linear ancestry. The effect of ancestry in this *post hoc* test represents

690　　　the post-peak ancestry effect, whereas the estimates of the interaction term represent the pre-

691　　　peak effect as a deviation from the post-peak ancestry effect[92,94]. The sum of the two

692　　　represents the pre-peak ancestry effect. After scaling all variables to aid model convergence,

693　　　we ran all the above models on five chains, each with 5500 iterations (500 warm-up) and

694　　　maximal tree depth set to 15.

695

696　　　*Testing for character displacement in rhythm*

697　　　We also hypothesized that if divergent character displacement through reinforcement has a

698　　　stabilizing effect on IOI, then pure ancestry individuals in the contact zone are expected to

699　　　have more stable songs than individuals in allopatry. We added acoustic data from recordings

700　　　of 59 unbanded *extoni* and 38 *pusillus* individuals from distant allopatry and assumed *pusillus*

701　　　ancestry of 0 and 1 respectively for *extoni* and *pusillus* based on estimated Q values from

702　　　fastSTRUCTURE of 83 *extoni* (0.01±0.1) and 24 *pusillus* (0.99±0.003) from allopatric

703　　　populations. We fitted a model on the resulting dataset of 181 individuals with ancestry

704　　　estimates Q < 0.01 for *extoni* (n = 87) and Q > 0.99 for *pusillus* (n = 94), incorporating 84

705　　　individuals with ancestry values estimated in fastSTRUCTURE. We used standardized IOI as

706　　　the response variable in DHGLMs, and included species, population (categorical with two

707　　　levels: allopatric vs. sympatric) and their interaction, as fixed factors, with individual ID used

708　　　as a random factor. This structure was used in both the 'mean' and the 'RWV' parts of the

709 model. For these models, we ran five chains over 7500 iterations (750 warm-up) and the

710 maximal tree depth was set to 15. Model convergence and chain mixing for all the above-

711 mentioned models were evaluated using the *Rhat* estimates and by graphical inspection of the

712 trace plots.

713

Acknowledgments

Author contributions:

728 Conceptualization: MS, AB, BvH, ANGK

729 Methodology: MS, SML, SS, AH, ND, EDJ, AB, BvH, ANGK

730 Genome assembly and curation: BH, JM, JB, SP, WC, OF, EDJ

731 Fieldwork planning and logistics: CTD, AM, ANGK

732 Fieldwork: SML, MS, AM, AB, ANGK

733 Molecular labwork: MM, CN

734 Investigation: MS, SML, SS, SGdS, AB, BvH, ANGK

735 Visualization: MS, SS

736 Funding acquisition: ANGK, MS, SML

Project administration: ANGK

Supervision: ANGK, AB, BvH

Writing – original draft: MS, SS, BvH, AB, ANGK

Writing – review & editing: All authors

Competing interests: Authors declare that they have no competing interests.

Data and materials availability: Scripts used for the analyses are available from https://github.com/MatteoSebastianelli/Tinkerbird_SongGene. Associated data are available under GenBank accession numbers GCA_015220805.1 and GCA_015220175.1, BioProject accession number PRJNA987636 and on Dryad (DOI: 10.5061/dryad.612jm6485).

References and Notes

1. Catchpole, C. K. & Slater, P. J. B. *Bird Song: Biological Themes and Variations*. (Cambridge University Press, 2008).

2. Roeske, T. C., Tchernichovski, O., Poeppel, D. & Jacoby, N. Categorical Rhythms Are Shared between Songbirds and Humans. *Curr. Biol.* **30**, 3699 (2020).

3. Ravignani, A., Bowling, D. L. & Fitch, W. T. Chorusing, synchrony, and the evolutionary functions of rhythm. *Front. Psychol.* **5**, 1118 (2014).

4. Kotz, S. A., Ravignani, A. & Fitch, W. T. The Evolution of Rhythm Processing. *Trends Cogn. Sci.* **22**, 896–910 (2018).

5. Lambrechts, M. & Dhondt, A. A. The anti-exhaustion hypothesis: a new hypothesis to explain song performance and song switching in the great tit. *Anim. Behav.* **36**, 327–334 (1988).

6. Jiang, Y., Bolnick, D. I. & Kirkpatrick, M. Assortative mating in animals. *Am. Nat.* **181**, E125–38 (2013).

7. Servedio, M. R. Geography, assortative mating, and the effects of sexual selection on speciation with gene flow. *Evol. Appl.* **9**, 91–102 (2016).

8. Qvarnström, A., Haavie, J., Saether, S. A., Eriksson, D. & Pärt, T. Song similarity predicts hybridization in flycatchers. *J. Evol. Biol.* **19**, 1202–1209 (2006).

764   9.   Uy, J. A. C., Irwin, D. E. & Webster, M. S. Behavioral Isolation and Incipient Speciation in

765   Birds. *Annu. Rev. Ecol. Evol. Syst.* **49**, 1–24 (2018).

766   10.   Turbek, S. P. *et al.* Rapid speciation via the evolution of pre-mating isolation in the Iberá

767   Seedeater. *Science* **371**, (2021).

768   11.   Pfenning, A. R. *et al.* Convergent transcriptional specializations in the brains of humans and

769   song-learning birds. *Science* **346**, 1256846 (2014).

770   12.   Cahill, J. A. *et al.* Positive selection in noncoding genomic regions of vocal learning birds is

771   associated with genes implicated in vocal learning and speech functions in humans. *Genome Res.*

772   **31**, 2035–2049 (2021).

773   13.   Nwankwo, E. C. *et al.* Rampant introgressive hybridization in Pogoniulus tinkerbirds

774   (Piciformes: Lybiidae) despite millions of years of divergence. *Biol. J. Linn. Soc. Lond.* **127**,

775   125–142 (2019).

776   14.   Kirschel, A. N. G. *et al.* CYP2J19 mediates carotenoid colour introgression across a natural

777   avian hybrid zone. *Mol. Ecol.* **29**, 4970–4984 (2020).

778   15.   Toews, D. P. L. *et al.* Plumage Genes and Little Else Distinguish the Genomes of Hybridizing

779   Warblers. *Curr. Biol.* **26**, 2313–2318 (2016).

780   16.   Semenov, G. A. *et al.* Asymmetric introgression reveals the genetic architecture of a plumage

781   trait. *Nat. Commun.* **12**, 1019 (2021).

782   17.   Ryan, M. J. & Brenowitz, E. A. The Role of Body Size, Phylogeny, and Ambient Noise in the

783   Evolution of Bird Song. *American Naturalist* **126**, 87–100 (1985).

784   18.   Mikula, P. *et al.* A global analysis of song frequency in passerines provides no support for the

785   acoustic adaptation hypothesis but suggests a role for sexual selection. *Ecol. Lett.* **24**, 477–486

786   (2021).

787   19.   Sebastianelli, M., Lukhele, S. M., Nwankwo, E. C., Hadjioannou, L. & Kirschel, A. N. G.

788   Continent-wide patterns of song variation predicted by classical rules of biogeography. *Ecol.*

789   *Lett.* **25**, 2448–2462 (2022).

790   20.   Yang, J. *et al.* Genome partitioning of genetic variation for complex traits using common SNPs.

791   *Nat. Genet.* **43**, 519–525 (2011).

26

792   21. Suthers, R. A. & Zollinger, S. A. Producing song: the vocal apparatus. *Ann. N. Y. Acad. Sci.*

793   **1016**, 109–129 (2004).

794   22. Niarchou, M. *et al.* Genome-wide association study of musical beat synchronization

795   demonstrates high polygenicity. *Nat Hum Behav* **6**, 1292–1309 (2022).

796   23. De Gregorio, C. *et al.* Categorical rhythms in a singing primate. *Curr. Biol.* **31**, R1379–R1380

797   (2021).

798   24. Ravignani, A. & Madison, G. The Paradox of Isochrony in the Evolution of Human Rhythm.

799   *Front. Psychol.* **8**, 1820 (2017).

800   25. Rhie, A. *et al.* Towards complete and error-free genome assemblies of all vertebrate species.

801   *Nature* **592**, 737–746 (2021).

802   26. Rhie, A., Walenz, B. P., Koren, S. & Phillippy, A. M. Merqury: reference-free quality,

803   completeness, and phasing assessment for genome assemblies. *Genome Biol.* **21**, 245 (2020).

804   27. Simão, F. A., Waterhouse, R. M., Ioannidis, P., Kriventseva, E. V. & Zdobnov, E. M. BUSCO:

805   assessing genome assembly and annotation completeness with single-copy orthologs.

806   *Bioinformatics* **31**, 3210–3212 (2015).

807   28. de Oliveira, T. D. *et al.* Genomic Organization of Repetitive DNA in Woodpeckers (Aves,

808   Piciformes): Implications for Karyotype and ZW Sex Chromosome Differentiation. *PLoS One*

809   **12**, e0169987 (2017).

810   29. Houtgast, E. J., Sima, V.-M., Bertels, K. & Al-Ars, Z. Hardware acceleration of BWA-MEM

811   genomic short read mapping for longer read lengths. *Comput. Biol. Chem.* **75**, 54–64 (2018).

812   30. McKenna, A. *et al.* The Genome Analysis Toolkit: a MapReduce framework for analyzing next-

813   generation DNA sequencing data. *Genome Res.* **20**, 1297–1303 (2010).

814   31. Zhou, X. & Stephens, M. Genome-wide efficient mixed-model analysis for association studies.

815   *Nat. Genet.* **44**, 821–824 (2012).

816   32. Altschul, S. F., Gish, W., Miller, W., Myers, E. W. & Lipman, D. J. Basic local alignment search

817   tool. *J. Mol. Biol.* **215**, 403–410 (1990).

818   33. Kasem, E., Kurihara, T. & Tabuchi, K. Neurexins and neuropsychiatric disorders. *Neurosci. Res.*

819   **127**, 53–60 (2018).

820 34. Galosi, S. *et al.* Dystonia-Ataxia with early handwriting deterioration in COQ8A mutation

821 carriers: A case series and literature review. *Parkinsonism Relat. Disord.* **68**, 8–16 (2019).

822 35. Benítez-Burraco, A., Salud Jiménez-Romero, M. & Fernández-Urquiza, M. Delving into the

823 Genetic Causes of Language Impairment in a Case of Partial Deletion of *NRXN1*. *Molecular*

824 *Syndromology* vol. 13 496–510 Preprint at https://doi.org/10.1159/000524710 (2022).

825 36. Goffin, J. M. *et al.* Focal adhesion size controls tension-dependent recruitment of α-smooth

826 muscle actin to stress fibers. *J. Cell Biol.* **172**, 259–268 (2006).

827 37. Shahbazi, M. *et al.* Comprehensive association analysis of speech recognition thresholds after

828 cisplatin-based chemotherapy in survivors of adult-onset cancer. *Cancer Med.* (2022).

829 38. Uhlén, M. *et al.* Proteomics. Tissue-based map of the human proteome. *Science* **347**, 1260419

830 (2015).

831 39. Vitti, J. J., Grossman, S. R. & Sabeti, P. C. Detecting natural selection in genomic data. *Annu.*

832 *Rev. Genet.* **47**, 97–120 (2013).

833 40. Brooks, M. E., Kristensen, K. & Van Benthem, K. J. glmmTMB balances speed and flexibility

834 among packages for zero-inflated generalized linear mixed modeling. *The R journal* **9**, (2017).

835 41. Haavie, J. *et al.* Flycatcher song in allopatry and sympatry--convergence, divergence and

836 reinforcement. *J. Evol. Biol.* **17**, 227–237 (2004).

837 42. Sørensen, E. F. *et al.* Genome-wide coancestry reveals details of ancient and recent male-driven

838 reticulation in baboons. *Science* **380**, eabn8153 (2023).

839 43. Grayton, H. M., Missler, M., Collier, D. A. & Fernandes, C. Altered social behaviours in

840 neurexin 1α knockout mice resemble core symptoms in neurodevelopmental disorders. *PLoS*

841 *One* **8**, e67114 (2013).

842 44. Byers, J., Hebets, E. & Podos, J. Female mate choice based upon male motor performance. *Anim.*

843 *Behav.* **79**, 771–778 (2010).

844 45. Kirschel, A. N. G., Blumstein, D. T. & Smith, T. B. Character displacement of song and

845 morphology in African tinkerbirds. *Proc. Natl. Acad. Sci. U. S. A.* **106**, 8256–8261 (2009).

846 46. Kirschel, A. N. G., Nwankwo, E. C., Seal, N. & Grether, G. F. Time spent together and time

847 spent apart affect song, feather colour and range overlap in tinkerbirds. *Biol. J. Linn. Soc. Lond.*

848 **129**, 439–458 (2020).

849 47. Ravinet, M. *et al.* Interpreting the genomic landscape of speciation: a road map for finding

850   barriers to gene flow. *J. Evol. Biol.* **30**, 1450–1477 (2017).

851 48. Burchardt, L. S., Norton, P., Behr, O., Scharff, C. & Knörnschild, M. General isochronous

852   rhythm in echolocation calls and social vocalizations of the bat Saccopteryx bilineata. *R Soc*

853   *Open Sci* **6**, 181076 (2019).

854 49. Merker, B. H., Madison, G. S. & Eckerdal, P. On the role and origin of isochrony in human

855   rhythmic entrainment. *Cortex* **45**, 4–17 (2009).

856 50. Lukhele, S. M., Widdows, C. D. & Kirschel, A. N. G. Video evidence of song in a nestling

857   Yellow-rumped Tinkerbird (Pogoniulus bilineatus) supports innate song development in

858   Piciformes. *Wilson J. Ornithol.* **134**, 358–365 (2022).

859 51. Rouse, A. A., Patel, A. D. & Kao, M. H. Vocal learning and flexible rhythm pattern perception

860   are linked: Evidence from songbirds. *Proc. Natl. Acad. Sci. U. S. A.* **118**, (2021).

861 52. Soma, M. & Brumm, H. Group living facilitates the evolution of duets in barbets. *Biol. Lett.* **16**,

862   20200399 (2020).

863 53. K. Lisa Yang Center for Conservation Bioacoustics at the Cornell Lab of Ornithology. Ithaca,

864   NY: The Cornell Lab of Ornithology. Available from https://ravensoundsoftware.com/. *Raven*

865   *Pro: Interactive Sound Analysis Software (Version 1.6.4) [Computer software]*. (2023).

866 54. Sebastianelli, M., Blumstein, D. T. & Kirschel, A. N. G. Higher-pitched bird song towards the

867   coast supports a role for selection in ocean noise avoidance. *Bioacoustics* **31**, 41–58 (2021).

868 55. Slabbekoorn, H., Ellers, J. & Smith, T. B. Birdsong and Sound Transmission: The Benefits of

869   Reverberations. *Condor* **104**, 564–573 (2002).

870 56. Ravignani, A., Delgado, T. & Kirby, S. Musical evolution in the lab exhibits rhythmic

871   universals. *Nature Human Behaviour* **1**, 1–7 (2016).

872 57. Vurture, G. W. *et al.* GenomeScope: fast reference-free genome profiling from short reads.

873   *Bioinformatics* **33**, 2202–2204 (2017).

874 58. Chin, C.-S. *et al.* Nonhybrid, finished microbial genome assemblies from long-read SMRT

875   sequencing data. *Nat. Methods* **10**, 563–569 (2013).

876 59. Chin, C.-S. *et al.* Phased diploid genome assembly with single-molecule real-time sequencing.

877 *Nat. Methods* **13**, 1050–1054 (2016).

878 60. Guan, D. *et al.* Identifying and removing haplotypic duplication in primary genome assemblies.

879 *Bioinformatics* **36**, 2896–2898 (2020).

880 61. Formenti, G. *et al.* SMRT long reads and Direct Label and Stain optical maps allow the

881 generation of a high-quality genome assembly for the European barn swallow (Hirundo rustica

882 rustica). *Gigascience* **8**, (2019).

883 62. Ghurye, J. *et al.* Integrating Hi-C links with assembly graphs for chromosome-scale assembly.

884 *PLoS Comput. Biol.* **15**, e1007273 (2019).

885 63. Formenti, G. *et al.* Complete vertebrate mitogenomes reveal widespread gene duplications and

886 repeats. *Genome Biol* **22**, (2021).

887 64. Garrison, E. & Marth, G. Haplotype-based variant detection from short-read sequencing. *arXiv*

888 *[q-bio.GN]* (2012).

889 65. Howe, K. *et al.* Significantly improving the quality of genome assemblies through curation.

890 *Gigascience* **10**, (2021).

891 66. Chow, W. *et al.* gEVAL — a web-based browser for evaluating genome assemblies.

892 *Bioinformatics* **32**, 2508–2510 (2016).

893 67. Harry, E. *PretextView (Paired REad TEXTure Viewer): A desktop application for viewing*

894 *pretext contact maps. 2022;(Accessed: 19 October 2022).* (2022).

895 68. Formenti, G. *et al.* Gfastats: conversion, evaluation and manipulation of genome sequences using

896 assembly graphs. *bioRxiv* 2022.03.24.485682 (2022) doi:10.1101/2022.03.24.485682.

897 69. Community, T. G. *et al.* The Galaxy platform for accessible, reproducible and collaborative

898 biomedical analyses: 2022 update. *Nucleic Acids Research* Preprint at

899 https://doi.org/10.1093/nar/gkac247 (2022).

900 70. Secomandi, S. *et al.* A chromosome-level reference genome and pangenome for barn swallow

901 population genomics. *Cell Rep.* **42**, 111992 (2023).

902 71. Morgulis, A., Gertz, E. M., Schäffer, A. A. & Agarwala, R. WindowMasker: window-based

903 masker for sequenced genomes. *Bioinformatics* **22**, 134–141 (2006).

904   72.   Tarailo-Graovac, M. & Chen, N. Using RepeatMasker to identify repetitive elements in genomic

905   sequences. *Curr. Protoc. Bioinformatics* **Chapter 4**, Unit 4.10 (2009).

906   73.   Bao, W., Kojima, K. K. & Kohany, O. Repbase Update, a database of repetitive elements in

907   eukaryotic genomes. *Mob. DNA* **6**, 11 (2015).

908   74.   Martin, M. Cutadapt removes adapter sequences from high-throughput sequencing reads.

909   *EMBnet.journal* **17**, 10–12 (2011).

910   75.   Li, H. *et al.* The Sequence Alignment/Map format and SAMtools. *Bioinformatics* **25**, 2078–2079

911   (2009).

912   76.   Institue, B. Picard tools—by broad institute. Preprint at (2018).

913   77.   Danecek, P. *et al.* The variant call format and VCFtools. *Bioinformatics* **27**, 2156–2158 (2011).

914   78.   Catchen, J., Hohenlohe, P. A. & Bassham, S. Stacks: an analysis tool set for population

915   genomics. *Molecular* (2013).

916   79.   Purcell, S. *et al.* PLINK: a tool set for whole-genome association and population-based linkage

917   analyses. *Am. J. Hum. Genet.* **81**, 559–575 (2007).

918   80.   Alexander, D. H., Novembre, J. & Lange, K. Fast model-based estimation of ancestry in

919   unrelated individuals. *Genome Res.* **19**, 1655–1664 (2009).

920   81.   Raj, A., Stephens, M. & Pritchard, J. K. fastSTRUCTURE: variational inference of population

921   structure in large SNP data sets. *Genetics* **197**, 573–589 (2014).

922   82.   Guan, Y. Detecting structure of haplotypes and local ancestry. *Genetics* **196**, 625–642 (2014).

923   83.   Delaneau, O., Marchini, J. & Zagury, J.-F. A linear complexity phasing method for thousands of

924   genomes. *Nat. Methods* **9**, 179–181 (2011).

925   84.   Gautier, M., Klassmann, A. & Vitalis, R. rehh 2.0: a reimplementation of the R package rehh to

926   detect positive selection from haplotype structure. *Mol. Ecol. Resour.* **17**, 78–90 (2017).

927   85.   Derryberry, E. P., Derryberry, G. E., Maley, J. M. & Brumfield, R. T. HZAR: hybrid zone

928   analysis using an R software package. *Mol. Ecol. Resour.* **14**, 652–663 (2014).

929   86.   Fitzpatrick, B. HIest: Hybrid index estimation. Preprint at https://CRAN.R-

930   project.org/package=HIest (2013).

931   87.   Hartig, F. DHARMa: residual diagnostics for hierarchical (multi-level/mixed) regression models.

932 *R package version 0.3* (2019).

88. Lee, Y. & Nelder, J. A. Double hierarchical generalized linear models (with discussion). *J. R. Stat. Soc. Ser. C Appl. Stat.* **55**, 139–185 (2006).

89. Bürkner, P.-C. Brms: An R package for Bayesian multilevel models using Stan. *J. Stat. Softw.* **80**, (2017).

90. Lansverk, A. L. *et al.* The variability of song variability in zebra finch (Taeniopygia guttata) populations. *R Soc Open Sci* **6**, 190273 (2019).

91. Bates, D., Mächler, M., Bolker, B. & Walker, S. Fitting Linear Mixed-Effects Models using lme4. *arXiv [stat.CO]* (2014).

92. Bouwhuis, S., Sheldon, B. C., Verhulst, S. & Charmantier, A. Great tits growing old: selective disappearance and the partitioning of senescence to stages within the breeding cycle. *Proc. Biol. Sci.* **276**, 2769–2777 (2009).

93. Bronshtein, I. N., Semendyayev, K. A., Musiol, G. & Mühlig, H. *Handbook of Mathematics*. (Springer, 2015).

94. Dingemanse, N. J., Moiron, M., Araya-Ajoy, Y. G., Mouchet, A. & Abbey-Lee, R. N. Individual variation in age-dependent reproduction: Fast explorers live fast but senesce young? *J. Anim. Ecol.* **89**, 601–613 (2020).

95. Gu, Z., Gu, L., Eils, R., Schlesner, M. & Brors, B. circlize Implements and enhances circular visualization in R. *Bioinformatics* **30**, 2811–2812 (2014).

Figures
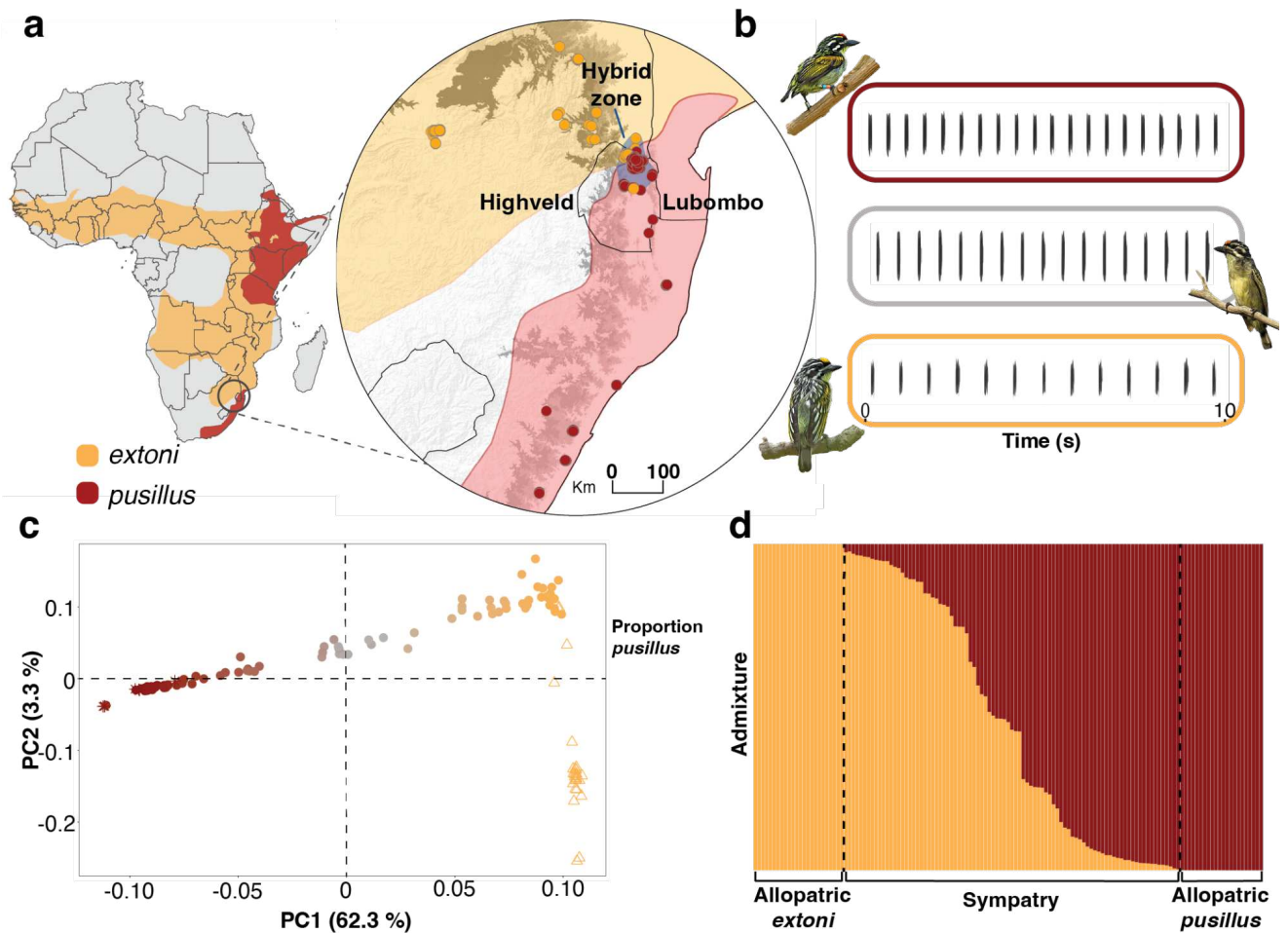
Fig. 1. Distribution, phenotype and hybridization patterns of yellow-fronted (*extoni*) and red-fronted tinkerbird (*pusillus*), (**a**) Geographic distribution of *extoni* (yellow) and *pusillus* (red) across Africa, with insert focusing on narrow hybrid zone (blue shading) channeled between the western highlands (highveld) and Lubombo mountains. Circles represent sampling localities of 452 tinkerbirds, with colors representing species according to forecrown color. (**b**) Spectrograms of tinkerbird song, illustrating rhythmic rate differences between individuals of the two species and intermediate song in a hybrid (gray border). (**c**) Whole-genome PCA, color-coded by ancestry with gray representing admixed individuals, and (**d**) ADMIXTURE plot (K = 2), together reveal the extent of mixed ancestry in the contact zone.
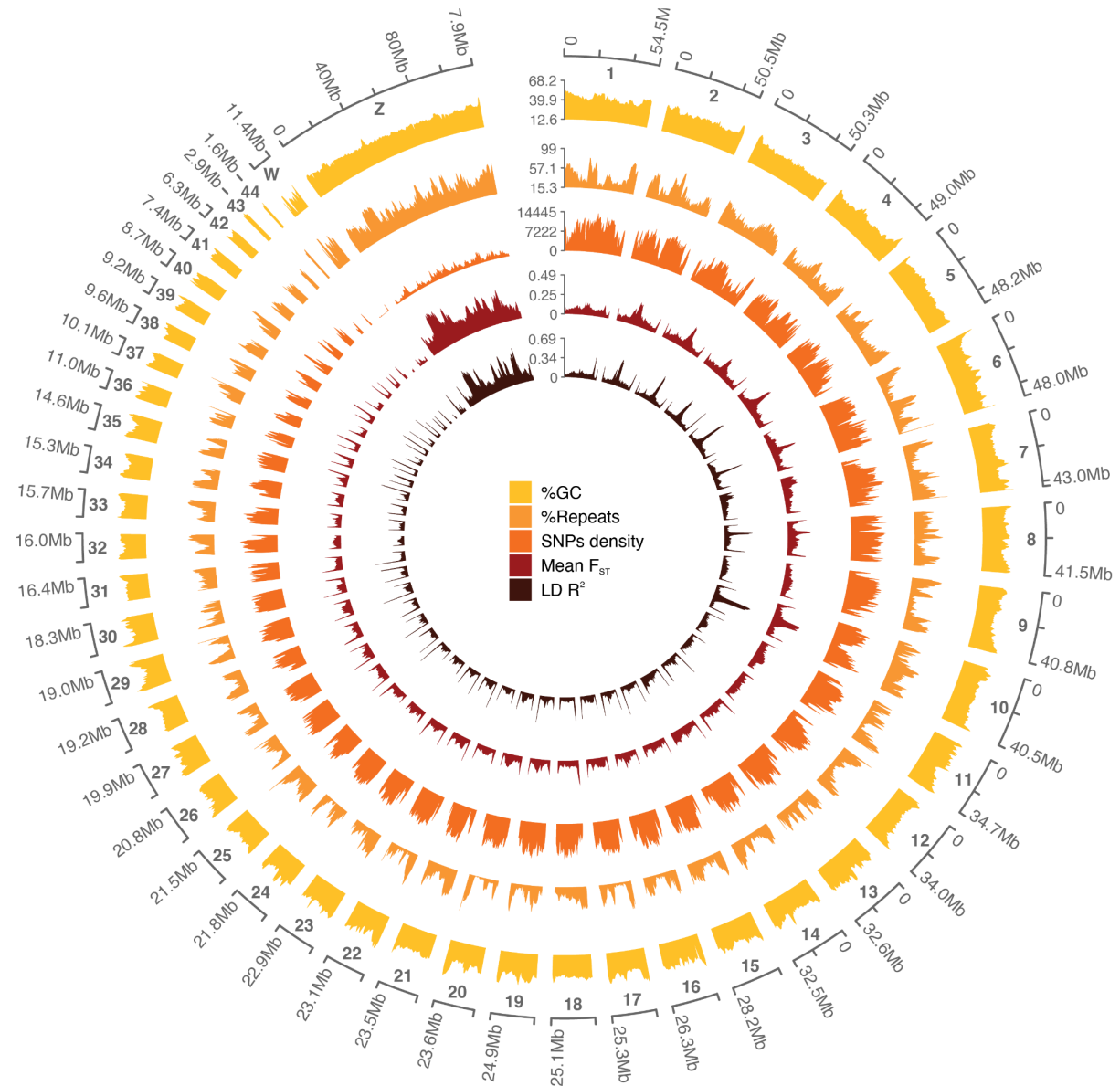
Fig. 2. The *pusillus* reference genome. Circos [95] plot representing the reference genome chromosomes. Data is plotted using 500 kbp windows. For each window, the percentage of G and C bases (%GC), the percentage or bases masked with Windowmasker and Repeatmasker (%Repeats), the number of SNPs (SNP density), the mean F_{ST} value (mean F_{ST}) and the mean LD value (LD (R^2)) is reported.
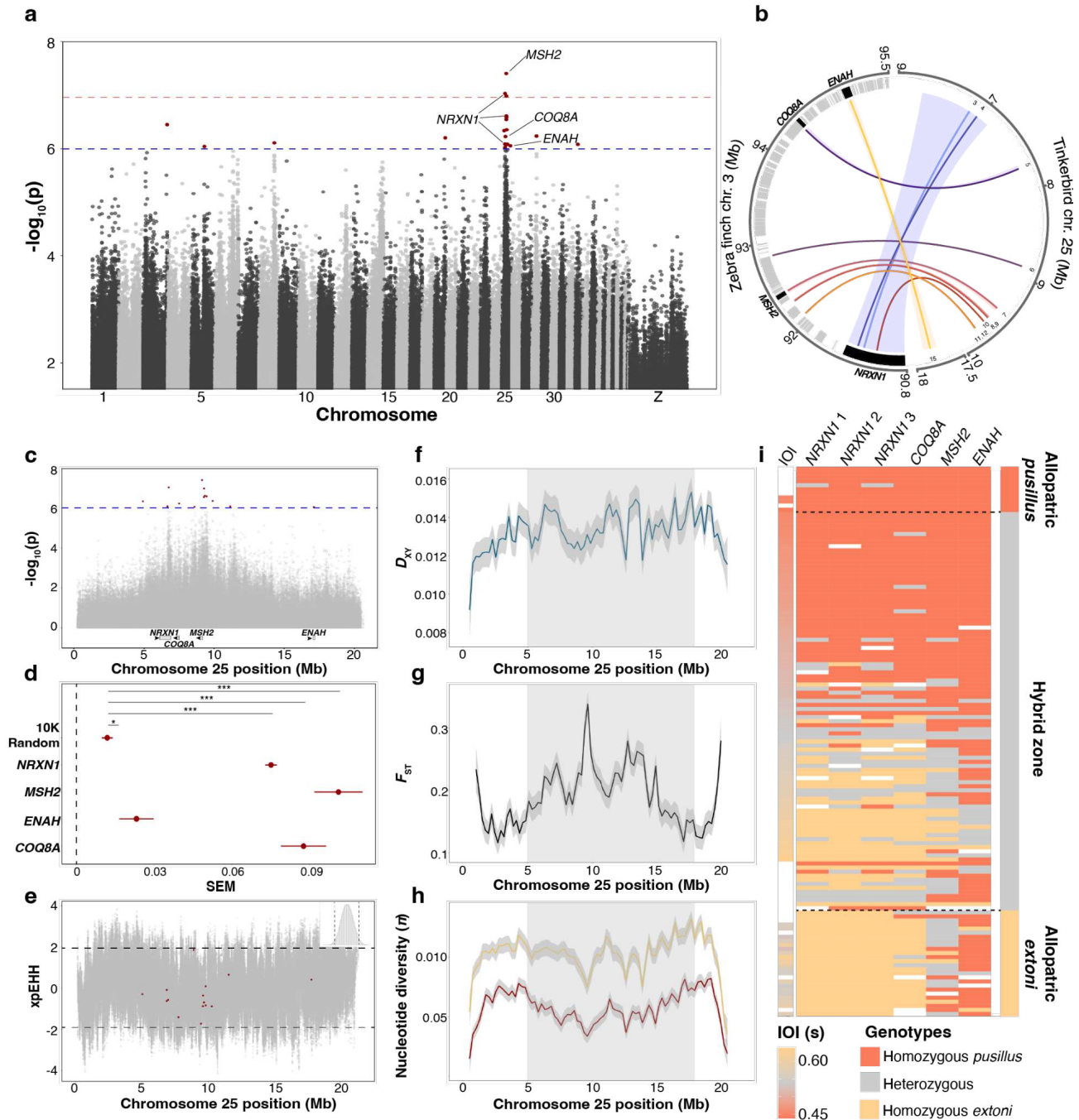
**Fig. 3. Candidate genes & genomic scans for signatures of selection and diversity.** (**a**) Manhattan
plot showing regions of the genome significantly associated with IOI, with red dots illustrating
significant SNPs and dashed lines the significance thresholds. Significant SNPs located on four
candidate genes are highlighted. (**b**) A close-up of chr. 25 illustrates the exact location where the 15
significant SNPs map on chromosome 3 of the zebra finch (thin link lines). The zebra finch genes
falling in the region are represented with gray squares. The four candidate genes are in black. Shaded
links represent the correspondence between the whole zebra finch gene and *pusillus* chr. 25. (**c**)
Location of significant SNPs (red dots) and candidate genes on chromosome 25. (**d**) The relative
contribution of significant SNPs to variance explained (Standard Error over the Mean - SEM). (**e**)
Main output of xpEHH on allopatric individuals, with 15 SNPs associated with IOI illustrated in red,
and positive (selection for *extoni*) and negative (selection for *pusillus*) significance thresholds.
Variation in (**f**) D_{XY} and (**g**) F_{ST}, and (**h**) comparison of **π** between the two species across chr. 25 (the
gray shaded area spans the range of the significant SNPs). (**i**) Candidate gene SNP genotypes across

138 individuals and associated IOI for those individuals whose songs were recorded. Note that
diversity statistics in (**e-h**) refer to allopatric individuals only.
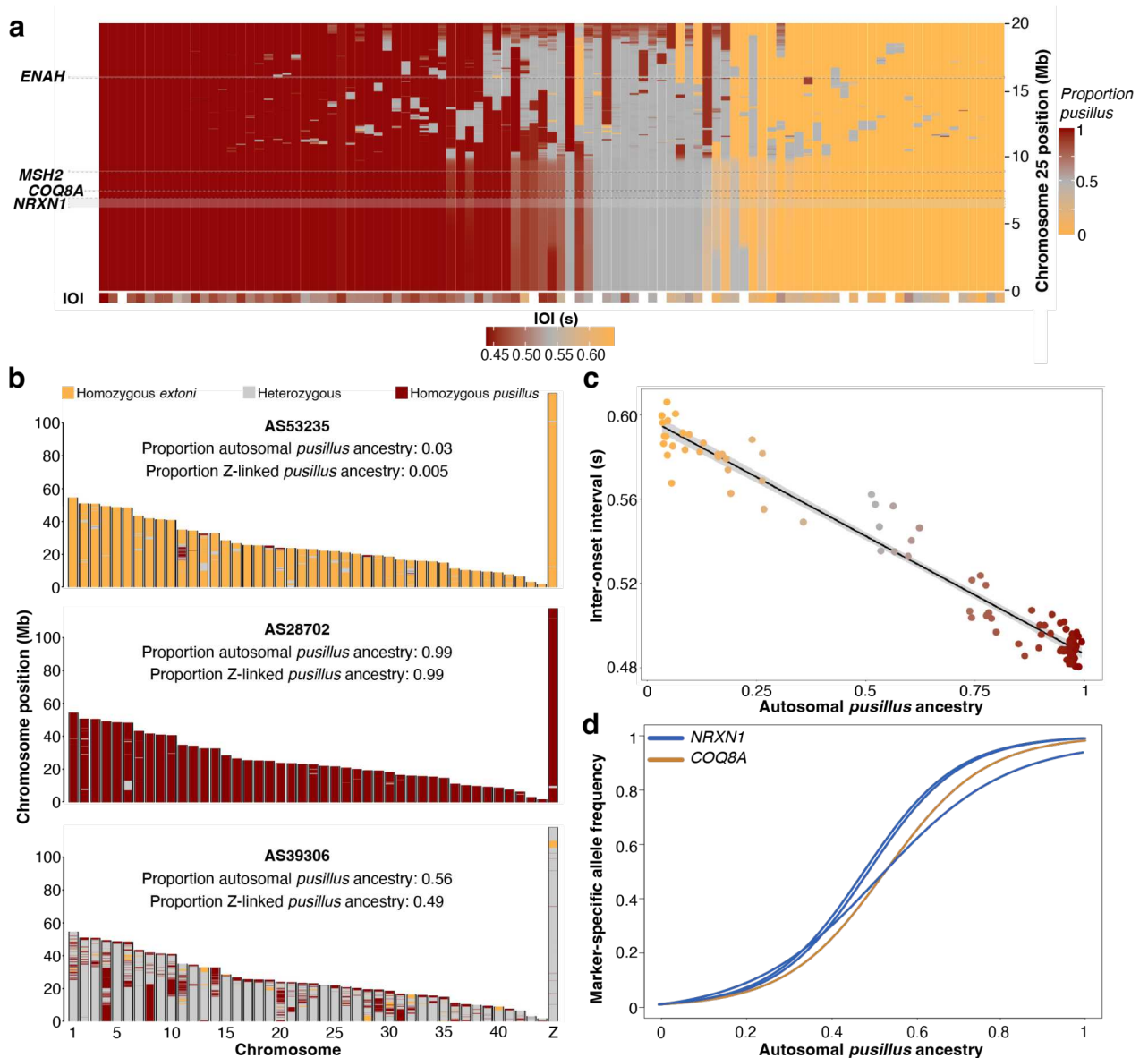
Fig. 4. The ancestry mosaicism of hybrid genomes. Ancestry block mosaicism illustrated (**a**) across
chromosome 25 of hybrid zone individuals (vertical bars organized left to right from the most *pusillus*
to the most *extoni* at chromosome 25) with respective IOI and (**b**) across the entire genome of mostly
one or other parental species and admixed ancestries, and the association of such variability in
ancestry (**c**) with IOI, where the black line represent the regression line of a linear mixed model (see
Methods) and dots represent raw data color-coded by ancestry (following the color-scheme used for
pusillus ancestry in panel **a**). (**d**) Genomic clines on *NRXN1* and *COQ8A* illustrate shifts in allele
frequency of markers mapping onto candidate genes in relation to autosomal ancestry.
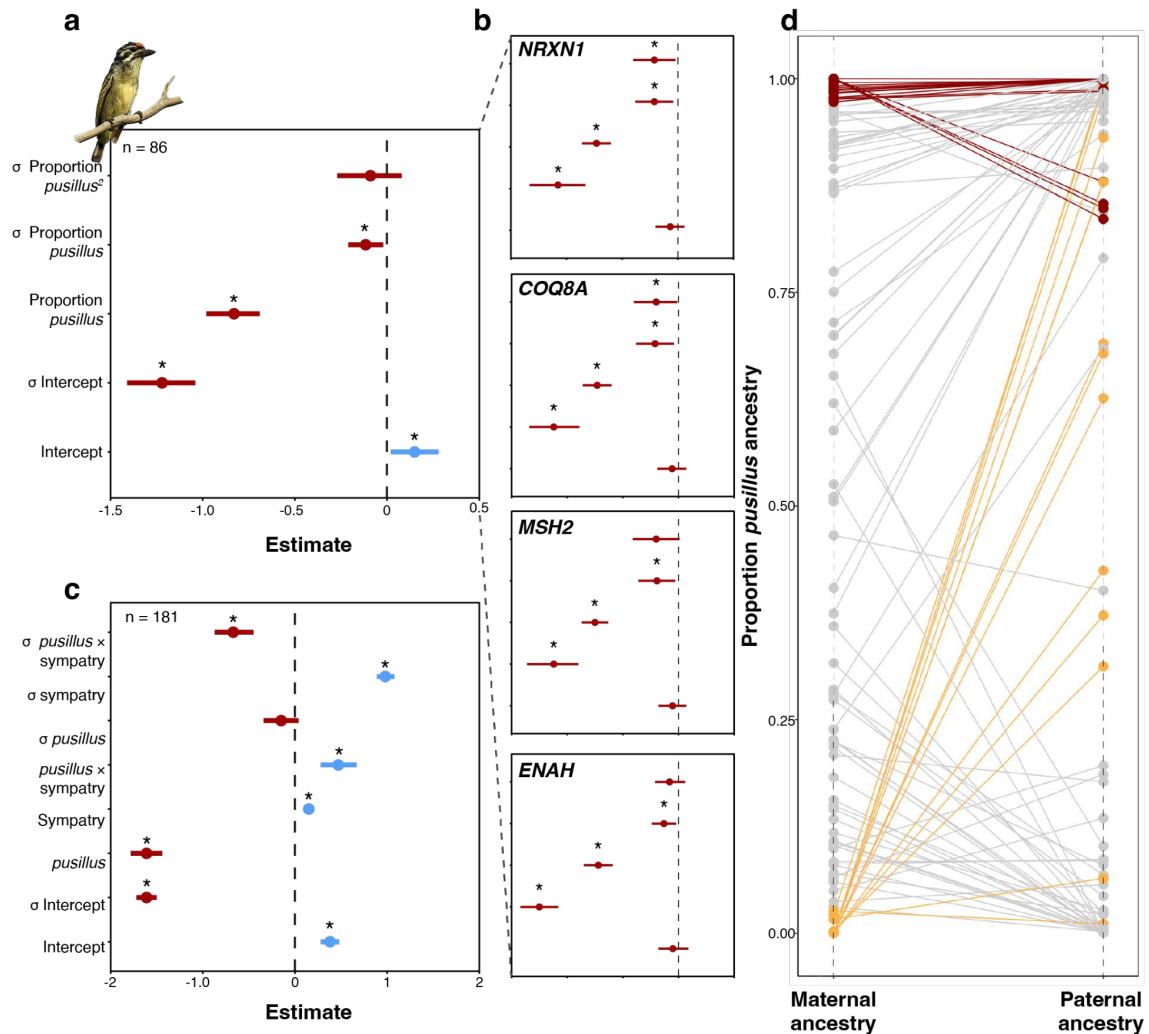
36

999
1000 **Fig. 5. Hybrid song instability, character displacement and asymmetric introgression.** Double-
1001 hierarchical linear mixed model results illustrating (**a**) genome-wide ancestry effects on IOI and its
1002 variance, with higher *pusillus* ancestry associated with faster, and more stable songs, with hypothesis
1003 of unstable songs in hybrids (H1) supported for those individuals with mixed ancestry (represented by
1004 quadratic term) specifically at (**b**) *NRXN1* and *COQ8A* (smaller panels). Support for character
1005 displacement (**c**) in song stability (H2) in pure parental species ancestry individuals (> 99%), based on
1006 significant interaction of species (*pusillus*) and sympatry showing that the difference in stability
1007 between the species is significantly greater in sympatry (represented by σ *pusillus* x sympatry) than in
1008 allopatry (represented by σ *pusillus*), where it is not significantly different. σ terms indicate estimates
1009 for the variance part of the models, with * denoting statistically significant effects. Positive estimates
1010 and 95% CI represented in blue, negative in red. Parental ancestries (**d**) of 95 females (heterogametic
1011 sex) in the contact zone, determined by assigning Z chromosome ancestry to fathers and calculating
1012 proportion of the autosomal ancestry estimate attributed to mothers after accounting for paternal
1013 ancestry estimates. Pure *pusillus* mothers (> 0.97 *pusillus* ancestry, red lines) mate assortatively with
1014 (< 0.8) *pusillus* fathers, but pure *extoni* mothers (< 0.03 *pusillus* ancestry, yellow lines) mate with
1015 males across the spectrum of *pusillus* ancestry.
1016

37

Supplementary Files

This is a list of supplementary files associated with this preprint. Click to download.

- MSSongGeneSupplementaryMaterials.pdf
- extoni14Nov21.mp4
- pusillus23Nov21.mp4
- Hybridtinkerbird24Nov18.mp4